Defects in graphene: A topological description

Amit Goft,[1] Yuval Abulafia,[1] Nadav Orion,[1] Claude L. Schochet,[2] and Eric Akkermans[1]
[1]*Department of Physics, Technion – Israel Institute of Technology, Haifa 3200003, Israel*
[2]*Department of Mathematics, Technion – Israel Institute of Technology, Haifa 3200003, Israel*

(Received 18 April 2023; revised 6 July 2023; accepted 12 July 2023; published 7 August 2023)

Specific types of spatial defects or potentials can turn monolayer graphene into a topological material. These topological defects are classified by a spatial dimension D and they are systematically obtained from the Hamiltonian by means of its symbol $\mathcal{H}(\boldsymbol{k},\boldsymbol{r})$, an operator which generalizes the Bloch Hamiltonian and contains all topological information. This approach, when applied to Dirac operators, allows to recover the tenfold classification of insulators and superconductors. The existence of a stable $\mathbb{Z}$ topology is predicted as a condition on the dimension D, similar to the classification of defects in thermodynamic phase transitions. Kekule distortions, vacancies, and adatoms in graphene are proposed as examples of such defects and their topological equivalence is discussed.

DOI: 10.1103/PhysRevB.108.054101

I. INTRODUCTION

The tenfold classification of insulators and superconductors generalizes the Dyson classification for disordered systems [1] and proposes a systematic scheme to identify topological features. It is based on antiunitary symmetries, time reversal (TRS) and particle-hole (PHS), the unitary chiral symmetry (CS), and the space dimension d of noninteracting systems of fermions [2,3]. For each symmetry class, topological properties are deduced from band structures of Bloch Hamiltonians using a homotopy group based on the powerful yet abstruse K-theory classifying fibre bundles hence topological structures [2,4]. The principle leading to this classification remains challenging, and it hinders the role played by defects and disorder. This latter aspect has been considered [5] and the tenfold classification has been modified, replacing d by

$$\delta \equiv d - D, \tag{1}$$

where the dimension D characterizes the spatial envelope of defects.

This paper offers an alternative approach in the spirit of defect classification in thermodynamic phase transitions [6]. Introducing the tunable dimension D, we show how to change topological features of a given symmetry class in the tenfold classification by creating spatial defects or textures. We mostly consider examples from the *BDI* symmetry class, essentially monolayer graphene, an always surprising system, whose Bloch Hamiltonian, gapless at Dirac points, displays the three symmetries (TRS, PHS, and CS). In two dimensions, this class is not topological (see Table I). Creating defects, e.g., atomic vacancies, adatoms, or modulated perturbations, we discuss the conditions on D, so as to turn monolayer graphene into a topological material with nonvanishing integer invariant (a Chern or a winding number [7,8]) and topologically protected (zero modes) edge states. We show that defects and textures can be grouped into universality classes characterized by 4 parameters: two dimensions (d, D) and two integers (p, q) counting the number of Dirac matrices assigned to a Hamiltonian with specific defects. With Eq. (22), we prove a necessary condition to observe topological features. This condition applies to the 8 real symmetry classes of Table I, and it allows to retrieve all $\mathbb{Z}$-integer classes. When applied to the *BDI* symmetry class, Eq. (22) indicates that graphene with a vacancy belongs to the same universality class as a Kekule distortion, a rich model which displays fractional charge, $\mathbb{Z}$ topology, and a clear illustration of the Atiyah-Singer index theorem [9–20]. Other results are summarized in Table II. The paper is organized as follows. In Sec. II we define the symbol of a Hamiltonian and discuss its topological content. In Sec. III, we use the symbol to constructively establish the tenfold classification. In Sec. IV, we present examples of topological defects. In Sec. V we relate topological invariant numbers to edge states using an index theorem. Section VI discusses the applicability conditions of the index theorem, while Sec. VII summarizes our results.

II. THE SYMBOL OPERATOR

The simplest situation where both TRS and PHS can be implemented is a two-band model. Translation symmetry and Bloch theorem allow the reduction of a tight binding Hamiltonian matrix H to a 2×2 Bloch Hamiltonian matrix $\mathcal{H}(\boldsymbol{k})$. The pseudomomentum $\boldsymbol{k}$ takes values in the Brillouin zone, a d-dimensional compact torus $\mathbb{T}^d$. The energy spectrum of H is retrieved from the band energy spectrum $E_n(\boldsymbol{k})$ of $\mathcal{H}(\boldsymbol{k})$ and the topological properties obtained from the Berry connection are encoded in the Bloch wavefunctions. The tenfold classification relies upon a generalization of this model using Clifford algebras of $n \times n$ anticommuting Dirac matrices. In the presence of a spatially varying and nonperiodic potential [5], we associate to a Hamiltonian $H(-i\nabla, \boldsymbol{r})$ its symbol $\mathcal{H}(\boldsymbol{k},\boldsymbol{r})$ defined by the Weyl transform [21,22]

$$\mathcal{H}(\boldsymbol{k},\boldsymbol{r}) = \int_{-\infty}^{\infty} d\boldsymbol{r}' e^{-i\boldsymbol{k}\cdot\boldsymbol{r}'} \left\langle \boldsymbol{r} + \frac{\boldsymbol{r}'}{2} \middle| H \middle| \boldsymbol{r} - \frac{\boldsymbol{r}'}{2} \right\rangle. \tag{2}$$

TABLE I. Tenfold classification. The first five columns display the 10 symmetry classes labeled by s and defined by their antiunitary symmetries T, P and chirality C. "+" ("−") means that the relevant operator is a symmetry which squares to 1 (−1) and "0" the absence thereof. The last 4 columns indicate possible topological classes $(0, \mathbb{Z}, \mathbb{Z}_2)$ as a function of the reduced dimension $\delta = d - D$.

Class	s	T	P	C	$\delta=0$	1	2	3
A	0	0	0	0	$\mathbb{Z}$	0	$\mathbb{Z}$	0
AIII	1	0	0	1	0	$\mathbb{Z}$	0	$\mathbb{Z}$
AI	0	+	0	0	$\mathbb{Z}$	0	0	0
BDI	1	+	+	1	$\mathbb{Z}_2$	$\mathbb{Z}$	0	0
D	2	0	+	0	$\mathbb{Z}_2$	$\mathbb{Z}_2$	$\mathbb{Z}$	0
DIII	3	-	+	1	0	$\mathbb{Z}_2$	$\mathbb{Z}_2$	$\mathbb{Z}$
AII	4	-	0	0	$2\mathbb{Z}$	0	$\mathbb{Z}_2$	$\mathbb{Z}_2$
CII	5	-	-	1	0	$2\mathbb{Z}$	0	$\mathbb{Z}_2$
C	6	0	-	0	0	0	$2\mathbb{Z}$	0
CI	7	+	-	1	0	0	0	$2\mathbb{Z}$

The symbol is routinely used when translation symmetry allows replacing $-i\partial_j$ by a wavenumber k_j, hence recovering the Bloch Hamiltonian, namely

$$\begin{aligned}\mathcal{H}(\boldsymbol{k}) &= \int_{-\infty}^{\infty} d\boldsymbol{r}'\, e^{-i\boldsymbol{k}\boldsymbol{r}'} \left\langle \boldsymbol{r} + \frac{\boldsymbol{r}'}{2} | H(\hat{k}) | \boldsymbol{r} - \frac{\boldsymbol{r}'}{2} \right\rangle \\ &= \frac{1}{2\pi} \int_{-\infty}^{\infty} d\boldsymbol{r}' d\boldsymbol{k}'\, e^{-i\boldsymbol{k}\boldsymbol{r}'} e^{i\boldsymbol{k}'\boldsymbol{r}'} H(\boldsymbol{k}') \\ &= \int_{-\infty}^{\infty} d\boldsymbol{k}' H(\boldsymbol{k}') \delta(\boldsymbol{k} - \boldsymbol{k}') \\ &= H(\boldsymbol{k}). \end{aligned} \tag{3}$$

The correspondence between a Hamiltonian and its symbol has been formalized [23, Chap. 24–27] and used to quantize classical systems by means of a Wigner transform

$$H(\hat{\boldsymbol{k}}, \hat{\boldsymbol{r}}) = \frac{1}{(2\pi)^2} \int_{-\infty}^{\infty} d\boldsymbol{a}\, d\boldsymbol{b}\, \tilde{\mathcal{H}}(\boldsymbol{a}, \boldsymbol{b})\, e^{i(\boldsymbol{a}\cdot\hat{\boldsymbol{r}} + \boldsymbol{b}\cdot\hat{\boldsymbol{k}})}, \tag{4}$$

where $\tilde{\mathcal{H}}(\boldsymbol{a}, \boldsymbol{b})$ is the Fourier transform of $\mathcal{H}(\boldsymbol{k}, \boldsymbol{r})$ with respect to $\boldsymbol{k}$ and $\boldsymbol{r}$. A Hamiltonian and its symbol do not generally share the same spectrum, e.g., a harmonic oscillator and its symbol have respectively a discrete (quantum) and a continuous (classical) spectra. Yet, in the presence of translation symmetry, a unitary transformation relates a Hamiltonian to its symbol, the Bloch Hamiltonian $\mathcal{H}(\boldsymbol{k})$, so that both can be used interchangeably. This state of affairs is the exception rather than the rule and although Bloch theorem does not apply when translation symmetry is broken, the symbol $\mathcal{H}(\boldsymbol{k}, \boldsymbol{r})$ is well defined. It does no longer provide information on the Hamiltonian spectrum, but it encodes all topological information [9–11], [23, Chap. 26–27]. Topologically invariant numbers can be retrieved from eigenfunctions of $\mathcal{H}(\boldsymbol{k}, \boldsymbol{r})$ provided a spectral gap exists in its eigenvalue spectrum. Note that the existence of this gap does not imply a similar behavior of the Hamiltonian except in the presence of translation symmetry. This remark is of utmost importance and it will become much clearer in the following example.

TABLE II. Defects fields in graphene. To display a $\mathbb{Z}$ topology (last column), the dimension D must fulfill $D = p + q - d$. V+A stands for vacancy + adatom.

	p	d	q	D	s	δ	Topology
Graphene	1	2	0	0	1	2	No
SSH	1	1	0	0	1	1	Yes
Vacancy	2	2	1	1	1	1	Yes
Kekule	2	2	1	1	1	1	Yes
Adatom	1	2	1	0	0	2	No
V + A	2	2	2	2	0	0	Yes

Graphene [24], a bipartite honeycomb lattice of carbon atoms well described by the Hamiltonian

$$H_0 = -t \sum_i \sum_{\delta=0}^{2} a_i^\dagger b_{i+\delta} + h.c., \tag{5}$$

with hopping t between nearest neighbors, provides a relevant playground to test these ideas. H_0 is diagonal in momentum space and its energy spectrum displays two independent Dirac points, K and K'. At low energy and in appropriate units, the Bloch Hamiltonian associated to H_0 is

$$\mathcal{H}_0(\boldsymbol{k}) = k_x\, \sigma_x \otimes \tau_z + k_y\, \sigma_y \otimes \mathbf{1} \tag{6}$$

in the sublattice basis $\psi_{\boldsymbol{k}} = (a_{\boldsymbol{k}}^K \quad a_{\boldsymbol{k}}^{K'} \quad b_{\boldsymbol{k}}^K \quad b_{\boldsymbol{k}}^{K'})^T$ with $\boldsymbol{k} = (k_x, k_y)$. In $\sigma_i \otimes \tau_j$, the Pauli matrix σ_i (resp. τ_j) corresponds to the sublattice (A, B) (resp. the valley K, K') degrees of freedom. The symbol [Eq. (6)] is invariant under antiunitary symmetries (TRS) and (PHS) and chiral symmetry $\{\mathcal{H}_0(\boldsymbol{k}), \sigma_z \otimes \mathbf{1}\} = 0$. Hence it belongs to the *BDI* class which, for $d = 2$, does not display topological features (see Table I).

Consider now creating a vacancy [25–32] by the removal of a neutral carbon atom located at the origin of the lattice. Hamiltonian Eq. (5) becomes

$$H_V = -t \sum_i \sum_{\delta=0}^{2} a_i^\dagger b_{i+\delta} + t \sum_{\delta=0}^{2} a_0^\dagger b_{0+\delta} + h.c. \tag{7}$$

The vacancy breaks translation symmetry so that $\boldsymbol{k}$ is no longer a good quantum number, but H_V can still be expanded at low energy around the Dirac points [33]

$$H_V = \int d\boldsymbol{r}\, \psi_{\boldsymbol{r}}^\dagger\, H(\boldsymbol{r}, -i\,\partial_{\boldsymbol{r}})\, \psi_{\boldsymbol{r}}. \tag{8}$$

Making use of the Weyl transform Eq. (2), we obtain the symbol

$$\begin{aligned}\mathcal{H}_V(\boldsymbol{k}, \boldsymbol{r}) = {} & k_x\, \sigma_x \otimes \tau_z + k_y\, \sigma_y \otimes \mathbf{1} \\ & + \phi_1(\boldsymbol{r}) \sigma_x \otimes \tau_x + \phi_2(\boldsymbol{r}) \sigma_x \otimes \tau_y, \end{aligned} \tag{9}$$

with $\boldsymbol{\phi}(\boldsymbol{r}) \equiv \phi_1 + i\phi_2 = \phi(r)\, e^{-i\theta}$, and θ being the angle relative to $\boldsymbol{r}$ (see Appendix A). A vacancy does not open a gap in the k-linear spectrum of H_V but it creates zero modes at the Fermi energy (for undoped graphene) and it couples the valleys [29,34,35]. However, the eigenvalue spectrum of the symbol [Eq. (9)] has a gap for any nonvanishing function $\phi(r) = (\phi_1^2 + \phi_2^2)^{1/2}$. This difference between a Hamiltonian and its symbol is displayed in Fig 1. Graphene with a vacancy

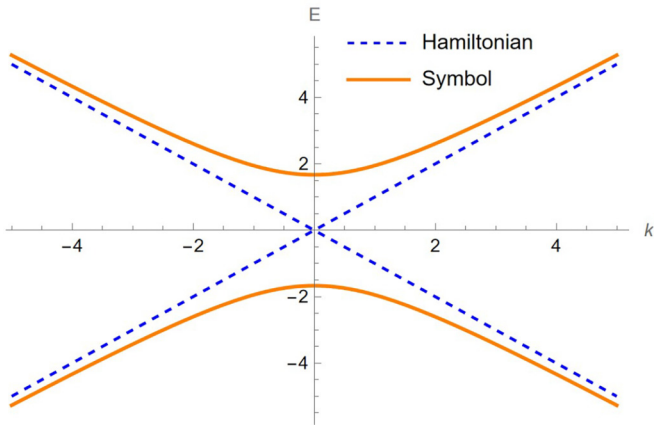

FIG. 1. Spectral behavior of graphene with a vacancy. The dashed line corresponds to the spectrum of the Hamiltonian H_V in Eq. (7). It is linear with $\boldsymbol{k}$ and gapless. The full line corresponds to the spectrum of the symbol [Eq. (9)] with $\phi(r) = \frac{1}{r \ln r/r_0}$.

does not have a spectral gap, hence it apparently does not belong to the tenfold classification. But its symbol has a gap and it is what matters for topological properties and the tenfold classification. This point is usually overlooked since in the presence of translation symmetry, a Hamiltonian and its symbol have related spectra.

Both H_V and $\mathcal{H}_V(\boldsymbol{k},\boldsymbol{r})$ are invariant under the antiunitary symmetries (TRS, PHS) and chiral symmetry $\{\mathcal{H}_V(\boldsymbol{k},\boldsymbol{r}), \sigma_z \otimes \mathbf{1}\} = 0$, so that graphene with a vacancy also belongs to *BDI*, seemingly void of topological features for $d = 2$. We wish to revisit that result.

III. BUILDING THE TENFOLD WAY WITH THE SYMBOL

We present an alternative derivation of the tenfold classification of insulators and superconductors based on properties of symbols $\mathcal{H}(\boldsymbol{k},\boldsymbol{r})$. We restrict our discussion to the 8 real symmetry classes displaying at least one of the antiunitary symmetries TRS or PHS. We recall for convenience that they are respectively described by $T = U_T K$ and $P = U_P K$, where U_T, U_P are unitary operators and K is the antiunitary complex conjugate. The chiral symmetry $C = TP = U_T U_P^*$ is their product. These symmetries translate for the symbols $\mathcal{H}(\boldsymbol{k},\boldsymbol{r})$ into the requirements

$$\begin{aligned} T\mathcal{H}(\boldsymbol{k},\boldsymbol{r})T^{-1} &= \mathcal{H}(-\boldsymbol{k},\boldsymbol{r}),\\ P\mathcal{H}(\boldsymbol{k},\boldsymbol{r})P^{-1} &= -\mathcal{H}(-\boldsymbol{k},\boldsymbol{r}),\\ C\mathcal{H}(\boldsymbol{k},\boldsymbol{r})C^{-1} &= -\mathcal{H}(\boldsymbol{k},\boldsymbol{r}). \end{aligned} \tag{10}$$

Table I accounts for symmetry classes of symbols $\mathcal{H}(\boldsymbol{k},\boldsymbol{r})$ of generic form

$$\mathcal{H}(\boldsymbol{k},\boldsymbol{r}) = \boldsymbol{h}_s \cdot \boldsymbol{\gamma}_s + \boldsymbol{h}_a \cdot \boldsymbol{\gamma}_a \equiv \boldsymbol{h}(\boldsymbol{k},\boldsymbol{r}) \cdot \boldsymbol{\gamma}. \tag{11}$$

The table extends to $\delta = 7$ and it is periodic both in s and δ. This constitutes Bott periodicity. For a discussion of this periodicity and its dependence on δ, we direct the reader to Ref. [5]. The set of anticommuting $\boldsymbol{\gamma}$ matrices is conveniently split into position and momentumlike $\boldsymbol{\gamma}_s$ and $\boldsymbol{\gamma}_a$ matrices according to Eq. (10), viz., symmetric $\boldsymbol{h}_s$ or antisymmetric $\boldsymbol{h}_a$ fields

$$\begin{aligned} \boldsymbol{h}_s(\boldsymbol{k},\boldsymbol{r}) &= \boldsymbol{h}_s(-\boldsymbol{k},\boldsymbol{r}), \quad T\gamma_s T^{-1} = \gamma_s,\\ \boldsymbol{h}_a(\boldsymbol{k},\boldsymbol{r}) &= -\boldsymbol{h}_a(-\boldsymbol{k},\boldsymbol{r}), \quad T\gamma_a T^{-1} = -\gamma_a. \end{aligned} \tag{12}$$

This implies

$$\begin{aligned} &[\gamma_s, T] = \{\gamma_a, T\} = 0,\\ &\{\gamma_s, P\} = [\gamma_a, P] = 0,\\ &\{\gamma_s, C\} = \{\gamma_a, C\} = 0. \end{aligned} \tag{13}$$

We denote p (resp. $q+1$) the number of γ_a (resp. γ_s) matrices. The momentum $\boldsymbol{k}$ depends on the spatial dimension d of the lattice and the position $\boldsymbol{r}$ which accounts for a potential breaking translation symmetry (hereafter a defect), is characterized by a dimension D. Hence symbols $\mathcal{H}(\boldsymbol{k},\boldsymbol{r})$ in Eq. (11) depend on the parameters (d, D, p, q) and are classified by $s = p - q \pmod 8$. A scaling relation

$$\mathcal{H}(d, D, p, q) = \mathcal{H}(s - \delta) \tag{14}$$

holds between s and $\delta \equiv d - D$ [5] (see Appendix B).

$\mathbb{Z}$-topology classes in Table I correspond to integer values of invariant integrals encoded in the eigenfunctions of the Bloch Hamiltonian. This result also holds for symbols $\mathcal{H}(\boldsymbol{k},\boldsymbol{r})$. The $(p+q+1)$-component field $\boldsymbol{h}(\boldsymbol{k},\boldsymbol{r})$ in Eq. (11) can be normalized $\hat{\boldsymbol{h}} = \boldsymbol{h}/h$ since the spectrum of the symbol has a gap ($h \neq 0$), hence we define

$$\hat{\mathcal{H}}(\boldsymbol{k},\boldsymbol{r}) = \hat{\boldsymbol{h}}(\boldsymbol{k},\boldsymbol{r}) \cdot \boldsymbol{\gamma}, \tag{15}$$

a procedure often called flattening. Each component $\hat{h}^i$ depends on $d + D$ variables, the d components $(k_1, \ldots, k_d)$ of $\boldsymbol{k}$ on the S^d sphere and the D spatial components $\boldsymbol{r} = (r_1, \ldots, r_D)$ of the defect, defined on S^D. For Dirac symbols [Eq. (11)], $\boldsymbol{\gamma}$ are $n \times n$ Dirac matrices with $n = 2^m$.

A. Topological Invariants

There exist two types of topologically invariant integers, depending on the parity of $d + D$. For even (odd) values, a Chern number $\mathcal{C}$ (a winding number ν) is defined to capture phase-space topological obstructions. They are expressed by the integrals

$$\mathcal{C}_m \propto \int_{S^{d+D}} \mathrm{Tr}[\hat{\mathcal{H}}(d\hat{\mathcal{H}})^{2m}], \tag{16}$$

where (Tr) is over the $\boldsymbol{\gamma}$ matrices and for chiral symbols $\hat{\mathcal{H}} = \hat{\boldsymbol{h}} \cdot \boldsymbol{\gamma} = \left(\begin{smallmatrix} 0 & \mathcal{Q} \\ \mathcal{Q}^\dagger & 0 \end{smallmatrix}\right)$,

$$\nu_{2m-1} \propto \int_{S^{d+D}} \mathrm{Tr}[(\mathcal{Q}^\dagger d\mathcal{Q})^{2m-1}]. \tag{17}$$

For nonchiral symbols, using the Clifford decomposition [Eq. (15)] $\hat{\mathcal{H}}(\boldsymbol{k},\boldsymbol{r}) = \hat{\boldsymbol{h}} \cdot \boldsymbol{\gamma}$, we have

$$\begin{aligned} \mathcal{C}_m &\propto \int \mathrm{Tr}[\hat{\mathcal{H}}(d\hat{\mathcal{H}})^{2m}]\\ &= \int \sum_{i_1, i_2, \cdots i_{2m+1}} h_{i_1} dh_{i_2} \cdots dh_{i_{2m+1}} \mathrm{Tr}\big[\gamma_{i_1}\gamma_{i_2}\cdots\gamma_{i_{2m+1}}\big]. \end{aligned} \tag{18}$$

This expression does not vanish for $i_2 \neq i_3 \neq \cdots \neq i_{2n+1}$, hence $\gamma_{i_2} \neq \gamma_{i_3} \neq \cdots \neq \gamma_{i_{2n+1}}$. A Dirac symbol without chiral

symmetry must be built out of all possible anticommuting γ matrices whose product is proportional to the identity. This implies that $\mathcal{C}_m$ in Eq. (18) does not vanish for $\gamma_{i_1} \neq \gamma_{i_2} \neq \gamma_{i_3} \neq \cdots \neq \gamma_{i_{2m+1}}$. Since γ matrices anticommute, exchanging indices will give relative $\pm$ signs depending on the exchanges, overall this expression gives complete antisymmetrization of all indices and is nothing but an integral of the Jacobian

$$J(\boldsymbol{h}, d, D) = \begin{vmatrix} h_1 & h_2 & \cdots & h_{d+D+1} \\ \partial_1 h_1 & \partial_1 h_2 & \cdots & \partial_1 h_{d+D+1} \\ \vdots & \vdots & \ddots & \vdots \\ \partial_{d+D} h_1 & \partial_{d+D} h_2 & \cdots & \partial_{d+D} h_{d+D+1} \end{vmatrix}, \quad (19)$$

provided we use the relation $2m = d + D$.

For chiral classes, we calculate a winding number written under the form

$$\begin{aligned} \nu_{2m-1} &\propto \int \mathrm{Tr}[(\mathcal{Q}^\dagger d\mathcal{Q})^{2m-1}] \\ &= (-1)^{m-1} \int \mathrm{Tr}[\mathcal{Q}^\dagger d\mathcal{Q} (d\mathcal{Q}^\dagger d\mathcal{Q})^{m-1}] \end{aligned} \quad (20)$$

where we have used the unitarity of $\mathcal{Q}$. In a basis where the symbol $\hat{\mathcal{H}} = \left(\begin{smallmatrix} 0 & \mathcal{Q} \\ \mathcal{Q}^\dagger & 0 \end{smallmatrix}\right) = \hat{\boldsymbol{h}} \cdot \boldsymbol{\gamma}$, one γ matrix is necessarily given either by $\gamma_1 = \sigma_x \otimes \mathbf{1}$ or $\gamma_1 = \sigma_y \otimes \mathbf{1}$ and the rest are given by $\gamma_i = \sigma_y \otimes \tilde{\gamma}_i$ or $\gamma_i = \sigma_x \otimes \tilde{\gamma}_i$ accordingly, where $\tilde{\gamma}_i$'s now define a complete set of anticommuting γ matrices. For simplicity, assume that $\gamma_1 = \sigma_y \otimes \mathbf{1}$, hence

$$\mathcal{Q} = -ih_1 \mathbf{1} + \sum_{i=2}^{2m-1} h_i \tilde{\gamma}_i \equiv \hat{\boldsymbol{h}} \cdot \tilde{\boldsymbol{\gamma}}, \quad (21)$$

a situation identical to the previous case of a Chern number. The product of all $\tilde{\gamma}$'s still being proportional to the identity matrix, the winding number is again proportional to an integral of the determinant [Eq. (19)], provided we use the relation $2m - 1 = d + D$. This determinant does not vanish only if the number of variables in $(\boldsymbol{k}, \boldsymbol{r})$ and in $\boldsymbol{h}$ are identical, namely if

$$d + D = p + q. \quad (22)$$

Overall, fixing a prefactor S_{d+D}, the surface of the unit sphere in $(d + D)$ dimensions, both Chern and winding numbers are given by an integral over the same determinant [Eq. (19)]:

$$\nu_{d+D} = \frac{1}{S_{d+D}} \int_{S^{d+D}} d^d k \, d^D r \, J(\boldsymbol{h}, d, D), \quad (23)$$

for all classes s and dimensions $(d + D)$. The only difference is that $d + D = 2m - 1$ for chiral classes, i.e., for odd values of $s = p - q$, while $d + D = 2m$ for nonchiral classes, i.e., for even values of s. This result can still be used for non normalized (flattened) symbols, provided we introduce a prefactor $(f^{d+D+1})^{-1}$ in the Jacobian, where

$$f = \sqrt{h_1^2 + h_2^2 + \cdots + h_{d+D+1}^2}. \quad (24)$$

To prove it, we note that a Dirac symbol is a superposition [Eq. (15)] of anticommuting γ matrices. Hence, it squares to the unit matrix up to the function f^2, so that to flatten a Dirac symbol one needs to divide it by f. The corresponding determinant is

$$\begin{vmatrix} \frac{h_1}{f} & \frac{h_2}{f} & \cdots & \frac{h_{d+D+1}}{f} \\ \partial_1 \frac{h_1}{f} & \partial_1 \frac{h_2}{f} & \cdots & \partial_1 \frac{h_{d+D+1}}{f} \\ \vdots & \vdots & \ddots & \vdots \\ \partial_{d+D} \frac{h_1}{f} & \partial_{d+D} \frac{h_2}{f} & \cdots & \partial_{d+D} \frac{h_{d+D+1}}{f} \end{vmatrix}. \quad (25)$$

Since each derivative is

$$\partial_i \frac{h_j}{f} = \frac{1}{f} \partial_i h_j - \frac{h_j}{f^2} \partial_i f, \quad (26)$$

and using the identity

$$\begin{vmatrix} a & b \\ c + e & d + f \end{vmatrix} = \begin{vmatrix} a & b \\ c & d \end{vmatrix} + \begin{vmatrix} a & b \\ e & f \end{vmatrix}, \quad (27)$$

the first term provides the result [Eq. (19)], while the second term vanishes since its rows are linearly dependent.

Relation Eq. (22) allows to identify $\mathbb{Z}$-topology classes for which either Chern or winding numbers may not vanish. It implies that $p + q$ and $d + D$ have the same parity, as well as $s = p - q$ and $\delta = d - D$. Hence, their difference $s - \delta$ must be even, namely odd values ensure the absence of $\mathbb{Z}$ topology. Moreover, under $\boldsymbol{k} \to -\boldsymbol{k}$, the determinant [Eq. (19)] is modified by an overall factor $(-1)^{d-p}$ of which d variables $\boldsymbol{k}$ for each derivative and p antisymmetric variables $\boldsymbol{h}_a$. Since Eq. (23) is evaluated over an even $\boldsymbol{k}$ domain, it vanishes for $d - p = 1 \pmod 2$. Noting that Eq. (22) implies $d - p = \frac{\delta - s}{2}$, we infer that for $\delta - s = 2 \pmod 4$, the corresponding classes do not have $\mathbb{Z}$ topology. Finally, the only classes with topological integer numbers correspond to

$$\delta - s \equiv 0 \pmod 4. \quad (28)$$

This result has been established otherwise by means of sophisticated methods [5]. Here, it is a direct consequence of properties of the Jacobian [Eq. (19)]. The novelty is in the introduction of D additional degrees of freedom which allow to change the number of symmetric $(\boldsymbol{h}_s)$ and antisymmetric $(\boldsymbol{h}_a)$ fields, hence modifying the scaling parameter $s - \delta$. The dimension D in Eq. (22) appears as a way to construct $\mathbb{Z}$-topological defect fields. To implement it, we consider Dirac symbols

$$\mathcal{H}(\boldsymbol{k}, \boldsymbol{r}) = \boldsymbol{k} \cdot \boldsymbol{\gamma_a} + \boldsymbol{\phi}(\boldsymbol{r}) \cdot \boldsymbol{\gamma_s}, \quad (29)$$

with linear momentum dependence and spatially dependent fields $\boldsymbol{\phi}(\boldsymbol{r})$. Evaluating Eq. (19) and integrating over $\boldsymbol{k}$ in Eq. (23), leads to

$$J(\boldsymbol{\phi}, D) = \begin{vmatrix} \phi_1 & \phi_2 & \cdots & \phi_{D+1} \\ \partial_1 \phi_1 & \partial_1 \phi_2 & \cdots & \partial_1 \phi_{D+1} \\ \vdots & \vdots & \ddots & \vdots \\ \partial_D \phi_1 & \partial_D \phi_2 & \cdots & \partial_D \phi_{D+1} \end{vmatrix} \quad (30)$$

so that $\nu_{d+D} = \nu_D$ and $\delta = s$ (the first $\mathbb{Z}$ diagonal in Table I). Relation Eq. (22) implies $d = p$ and $D = q$, therefore D ccharacterizes the defect fields $\boldsymbol{\phi}(\boldsymbol{r})$ in analogy with the defect classification in thermodynamic phase transitions [6]. A zero-dimensional defect, $D = q = 0$ corresponds to a real valued scalar field and a domain wall, $D = q = 1$ to a complex scalar field, $q = 2$ to a vector field, etc.

IV. TOPOLOGICAL DEFECTS

We now review examples summarized in Table II.

A. The SSH model

At low energies, the well-known SSH model [36,37] is described by the symbol

$$\mathcal{H}(k) = k\sigma_x + m\,\sigma_y, \tag{31}$$

characterized by $d = p = 1$ and $q = 0$. A position-dependent $m(\boldsymbol{r})$ does not change q. It corresponds to a real scalar field so that Eq. (22) requests $D = 0$ to display a nontrivial topology, i.e., a domain wall with winding number ± 1 [13].

B. Graphene with a vacancy

The Dirac symbol [Eq. (6)] of pristine monolayer graphene involves a pair (γ_s, γ_a) of Dirac matrices, so that $s = p - q = 1$. In the absence of defect field, namely for $\boldsymbol{\phi}(\boldsymbol{r}) = 0$, $D \equiv 0$ and $d + D = 2 \neq p + q = 1$. Hence Eq. (22) is not fulfilled and graphene does not display $\mathbb{Z}$ topology. Adding a vacancy, the corresponding symbol [Eq. (9)] fulfils Eq. (29). The vacancy field $\boldsymbol{\phi}(\boldsymbol{r})$ involves two symmetric γ_s, i.e., $p = 2, q = 1, d = 2$, and $s = 1$. Fulfilling Eq. (22) requires $D = 1$, so that $\boldsymbol{\phi}(\boldsymbol{r})$ is a complex valued field. All together, graphene with a vacancy belongs to the *BDI* class with $\delta = d - D = 1$, and a topological number calculated from Eqs. (23) and (30):

$$\nu_3 = \frac{1}{2\pi}\int dr\,\frac{1}{\phi_1^2+\phi_2^2}\begin{vmatrix}\phi_1 & \phi_2\\ \partial_r\phi_1 & \partial_r\phi_2\end{vmatrix} = \mp\int\frac{d\theta}{2\pi} = \mp 1, \tag{32}$$

which is the winding of the phase of $\boldsymbol{\phi}(\boldsymbol{r})$, encircling the vacancy, where $-1(+1)$ respectively corresponds to a vacancy on sublattice $A(B)$.

C. Graphene with an adatom

An adatom, another kind of spatial defect in graphene, shares several features with a vacancy, e.g., both have zero energy modes spatially located on the impurity, but they have distinct topological properties [38,39]. Unlike vacancies, creating an adatom involves a new energy scale which breaks particle-hole and chiral symmetries, suggesting it belongs to *AI* rather than *BDI* class. These features can be understood by adding to Eq. (6) a mass term

$$\mathcal{H}_A(\boldsymbol{k},\boldsymbol{r}) = h_1(\boldsymbol{k})\,\sigma_x + h_2(\boldsymbol{k})\,\sigma_y + m(\boldsymbol{r})\,\sigma_z, \tag{33}$$

where $h_1 - ih_2 = 1 + e^{-i\boldsymbol{k}\cdot\boldsymbol{a}_1} + e^{-i\boldsymbol{k}\cdot\boldsymbol{a}_2}$. Note that we only consider a single valley since the mass term does not couple the two valleys of graphene. Since $h_2(-k) = -h_2(k)$ and $h_1(-k) = h_1(k)$, the three Dirac matrices fulfill $p = 1$ and $q = 1$, so that $s = 0$ which indeed corresponds to the *AI* class. Relation Eq. (22) is satisfied for $D = 0$, implying $\delta = d - D = 2 \neq s$ so that graphene with an adatom does not display $\mathbb{Z}$ topology.

D. Graphene with vacancy and adatom

The coexistence of a vacancy and an adatom in graphene raises the experimentally relevant question of the topological prominence of a given defect field. The symbol of graphene, with a vacancy and an adatom at distinct locations, is of the type Eq. (29)

$$\mathcal{H}_{A+V}(\boldsymbol{k},\boldsymbol{r},\boldsymbol{r}') = \mathcal{H}_V(\boldsymbol{k},\boldsymbol{r}) + m(\boldsymbol{r}')\sigma_z\otimes\mathbf{1}. \tag{34}$$

It involves two fields, one complex and one scalar, so that $p = 2, q = 2$, and $s = 0$ (*AI* class). Relation Eq. (22) requests $D = 2$, namely an overall vector field for the combined defect (vacancy and adatom). Therefore, while the adatom breaks chiral symmetry $s = \delta = 0$, the vacancy + adatom system still displays $\mathbb{Z}$ topology. Since $d + D$ is even, from Eq. (30), the corresponding invariant is the second Chern number

$$\mathcal{C}_2 = \frac{1}{4\pi}\int dr dr'\,\frac{\partial_{r'}m}{\left(\phi_1^2+\phi_2^2+m^2\right)^{3/2}}\begin{vmatrix}\phi_1 & \phi_2\\ \partial_r\phi_1 & \partial_r\phi_2\end{vmatrix} = \mp 1. \tag{35}$$

E. Graphene with a Kekule distortion

Another defect field which came recently under scrutiny is the valley coupling Kekule distortion obtained by shifting the hopping term in Eq. (5) into $t_{\boldsymbol{r},i} = t + \delta t_{\boldsymbol{r},i}$ [40–44] with

$$\delta t_{\boldsymbol{r},i} = \Delta(\boldsymbol{r})\exp\left(i\boldsymbol{K}\cdot\boldsymbol{\delta}_i + i\Delta\boldsymbol{K}\cdot\boldsymbol{r}\right). \tag{36}$$

The corresponding symbol is Eq. (9) with $\boldsymbol{\phi}(\boldsymbol{r}) \equiv \Delta(\mathbf{r}) = \Delta_0(r)e^{i(\alpha+n\theta)}$ and constant α. The Kekule model and the vacancy are thus equivalent topological defects characterized by $D = 1$ (see Table II) and $\mathbb{Z}$ topology but with $\nu_3 = n$ instead of Eq. (32). The Kekule distortion exhibits topological fractional charge and so does a vacancy [27,35].

V. THE ATIYAH-SINGER INDEX THEOREM

A. Analytical and topological indices

The existence of $\mathbb{Z}$ topological defects is related to the appearance of zero energy modes in the spectrum of the Hamiltonian [45–47]. For a vacancy, this relation allows to calculate ν_{2m-1} in Eq. (17) using the Atiyah-Singer index theorem [9,10] relating properties of a Hamiltonian and its symbol. This theorem states that the analytical index, counting zero modes of an elliptic differential operator defined on compact manifolds, is equal to the topological index calculated from its symbol [23, Chap. 24–27]. Here, the elliptic differential operator is the Hamiltonian and the compact manifold is the Brillouin zone in the presence of translation symmetry or S^d otherwise. For a chiral Hamiltonian

$$H = \begin{pmatrix}0 & \mathcal{Q}\\ \mathcal{Q}^\dagger & 0\end{pmatrix}, \tag{37}$$

the analytical index is

$$\text{Index}\,H \equiv \dim\text{Ker}\,\mathcal{Q} - \dim\text{Ker}\,\mathcal{Q}^\dagger \tag{38}$$

and the topological index is the winding Eq. (17). For a vacancy in sublattice B (A), the Hamiltonian H_V in Eq. (7) is chiral, elliptic, and hosts a single zero mode located on sublattice A (B), hence its index is ± 1 as given by Eq. (32), and the Atiyah-Singer theorem becomes

$$\text{Index}\,H_V \equiv \dim\text{Ker}\,\mathcal{Q} - \dim\text{Ker}\,\mathcal{Q}^\dagger = \nu_3. \tag{39}$$

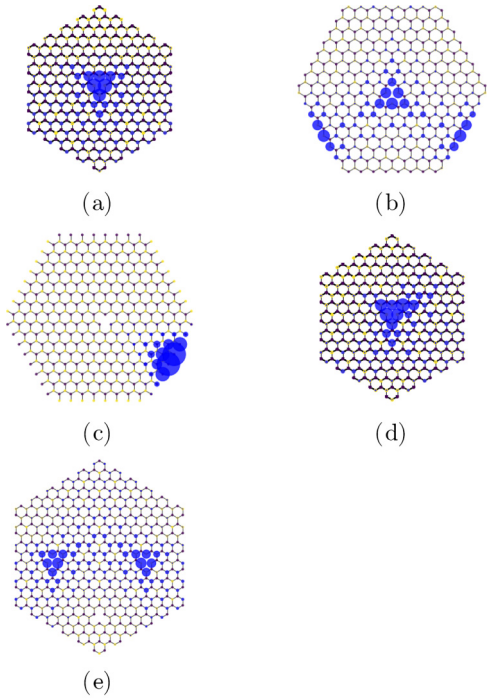

FIG. 2. Zero energy edge state from exact diagonalization of Eq. (7). (a), (b), and (c) correspond to armchair, zigzag, and bearded boundary conditions, (d) in the presence of disorder. (e) For three vacancies, two on the B sublattice and one on A, a single edge state is expected from Eq. (41) located on the majority B sublattice.

The index is still defined for a nonchiral Hamiltonian, e.g.,

$$H = \begin{pmatrix} M & \mathcal{Q} \\ \mathcal{Q}^\dagger & -M \end{pmatrix}, \tag{40}$$

where a mass term M shifts the energy spectrum. In that specific case, both the eigenstates and Index H remain unchanged but zero modes of $\mathcal{Q}$ and $\mathcal{Q}^\dagger$ belong to the spectrum only for a chiral Hamiltonian. For a space-dependent mass term, this illustrates what happens when adding an adatom to graphene with a vacancy. The adatom breaks chiral symmetry but preserves topology, viz., the index theorem [Eq. (39)] holds which relates the Chern number C_2 in Eq. (16) and the analytical index.

B. Bulk-Edge correspondence

Bulk-edge correspondence relates bulk topological numbers to edge states. For a vacancy with winding number ± 1, a single edge state is expected whose location depends on boundary conditions (Fig. 2). For any type of boundary conditions, the zero mode is located either on the edge of the lattice, on the vacancy location, or both. This suggests considering a vacancy as an additional edge of the lattice.

C. Generalization to finitely many vacancies

For any number (V_A, V_B) of vacancies, a generalization

$$\text{Index}\, H_V = V_A - V_B = \nu_3 \tag{41}$$

of the index theorem [Eq. (39)], allows to count edge states as shown in Fig. 2(e) for three vacancies, two on sublattice A and one on B, so that $\nu_3 = 1$, hence corresponding to a single edge state [35]. For a dimer and generally for $V_A = V_B$, $\nu_3 = 0$ and no edge state is expected despite the presence of vacancies.

D. Disorder

An important property of topological edge states is their robustness against perturbations, e.g., disorder. Introducing a random hopping term in Eq. (7), still preserves the topological zero energy edge state and its winding $\nu_3 = \mp 1$ as displayed in Fig. 2(d).

VI. APPLICABILITY OF INDEX THEOREMS

The Atiyah-Singer (AS) index theorem [9,10] is often invoked to identify zero energy states of a Hamiltonian as an edge (or boundary) mode and to relate them to topological (bulk) numbers. This procedure relating edge physics to bulk topological features constitutes the so-called bulk-edge correspondence. It is sometimes invoked improperly and it is the purpose of this section to discuss its relevance in more general terms using interesting and relevant limiting cases. The analytical index defined in Eq. (38),

$$\text{Index}\, H = \dim \text{Ker}\, \mathcal{Q} - \dim \text{Ker}\, \mathcal{Q}^\dagger, \tag{42}$$

characterises chiral Hamiltonians of the form Eq. (37). An important content of the AS theorem states that the number of zero modes counted by the analytical index is a topological invariant which can be expressed and related to the topological index of the symbol given either by a Chern or winding number. As appealing as it seems, it is important to pay attention to the strict applicability conditions of this theorem. It applies only to Fredholm operators or to elliptic differential operators defined on compact domains (hence a Fredholm operator). This class includes differential operators with invertible symbol namely having a gap, except for $\boldsymbol{k} = 0$ but with a finite multiplicity. Hence both zero modes counting spaces Ker $\mathcal{Q}$ and Ker $\mathcal{Q}^\dagger$ are finite dimensional. For example, the Laplacian is an elliptic differential operator whose symbol k^2 vanishes only at $\boldsymbol{k} = 0$. The Hamiltonian of graphene with a vacancy is also an elliptic differential operator as its symbol has a gap as given in Eq. (9) and displayed in Fig. 1.

Consider now two other systems, the nearest neighbors tight-binding model on a square lattice, essentially a discrete version of the Laplacian operator, and the Lieb lattice [48], both of which have zero energy modes and a chiral Hamiltonian of the form of Eq. (37). In both cases, the AS index theorem does not apply since the corresponding Hamiltonians are not elliptic differential operators. A square lattice displays apparent yet fictitious chiral symmetry. Although the lattice splits into two sublattices, this partition is unnecessary and misleading, since topological properties require exhausting all unitary symmetries. The symbol of the Hamiltonian of a square lattice, i.e., its Bloch Hamiltonian, is given by the function

$$\mathcal{H}_{SL} = -2t(\cos k_x a + \cos k_y a). \tag{43}$$

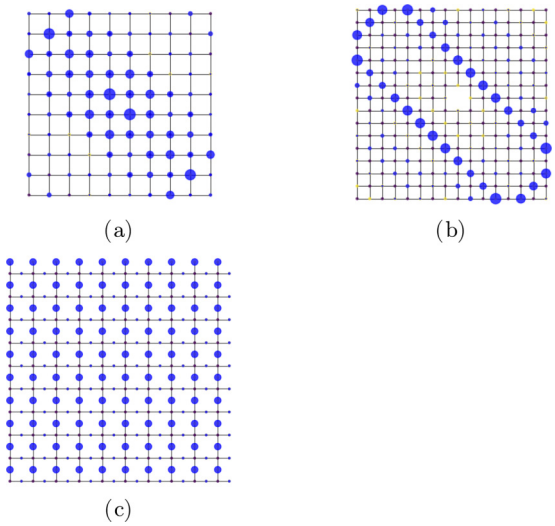

FIG. 3. Wavefunctions (squared) associated to zero modes (in blue) obtained by exact diagonalization of nearest-neighbor tight binding Hamiltonians. (a) A zero mode on a square lattice with Dirichlet boundary conditions. (b) A zero mode on a square lattice with Dirichlet boundary conditions and a single vacancy. (c) A zero mode on a Lieb lattice with periodic boundary conditions. These zero modes are not topological and they are not edge states.

This symbol vanishes along the lines $k_x \pm k_y = \pi$ and $k_x \pm k_y = -\pi$ so that the square lattice tight binding Hamiltonian is not elliptic. The low energy limit of the symbol (i.e., the Bloch Hamiltonian) of the Lieb lattice [48] Hamiltonian is given by

$$\mathcal{H}_L = -ta\, \boldsymbol{k} \cdot \boldsymbol{L}, \tag{44}$$

where

$$L_x = \begin{pmatrix} 0 & -i & 0 \\ i & 0 & 0 \\ 0 & 0 & 0 \end{pmatrix}, \quad L_y = \begin{pmatrix} 0 & 0 & -i \\ 0 & 0 & 0 \\ i & 0 & 0 \end{pmatrix}. \tag{45}$$

A diagonalization of $\mathcal{H}_L$ shows that this symbol has a single Dirac cone and a flat band of zero energy modes, hence it is also not elliptic.

Considering the topology of these two systems, we immediately check that the square lattice is not topological. It belongs to the *AI* class (see Table I) since the symbol (Bloch Hamiltonian) [Eq. (43)] has time reversal symmetry $T = K$ but no particle hole symmetry ($s = 0$) and it has $\delta = d - D = 2 - 0 = 2$, hence void of topological invariant numbers. Adding a vacancy to this system will still give trivial topology since $\delta = d - D = 2 - 1 = 1$. The Lieb lattice symbol [Eq. (44)] does not have gap and it cannot be expressed by means of Dirac matrices of a Clifford algebra, so that it does not belong to the tenfold classification. Yet, it may display topological features accessible from a version of the Atiyah Singer index theorem different from Eq. (39) [49]. This possibility is ruled out because index theorems apply to elliptic operators whose spectrum vanishes for finitely many eigenvalues [23], in contradiction with the existence of a zero energy flat band.

However, both Hamiltonians have zero modes displayed in Fig. 3. These zero modes are not of topological origin as the index theorem is not valid in these cases. Said otherwise, these zero modes are not edge states, they are not localized on the edges of the lattice, nor on the vacancy location, and they are not protected against perturbations, e.g., they are sensitive to disorder.

VII. CONCLUSION

We have introduced defect fields characterized by a dimension D and symbol operators generalizing Bloch Hamiltonians, to tailor topological features of materials describable by the tenfold classification. This approach should prove useful to use appropriate defects or textures to create quantum materials with topological features on demand, namely to allow navigating between different entries of the tenfold classification.

More specifically, we have considered valley-coupling defect fields $\boldsymbol{\phi}(\boldsymbol{r})$ in graphene or like materials. The existence of invariant numbers (Chern or winding) translate into edge states and their relation to powerful index theorems has been emphasized. Defect fields have been considered, e.g., vacancy and adatom which, despite common features, are not topologically akin. We have discussed examples where zero energy modes exist which are not related to any topological features, hence care is required when extrapolating results obtained in the framework of the tenfold classification.

ACKNOWLEDGMENTS

This work was supported by the Israel Science Foundation Grant No. 772/21 and by the Pazy Foundation.

APPENDIX A: SYMBOL OF GRAPHENE WITH A VACANCY

In this Appendix, we establish Eq. (9) for the symbol of graphene with a vacancy. Since topological obstructions if at all show up at any energy scale, it is sufficient to establish the expression of the symbol in the low energy limit. The low energy contribution of a vacancy in sublattice A to the tight binding Hamiltonian of graphene is given, in appropriate units, by the 4×4 matrix [33]

$$V(\boldsymbol{k}, \boldsymbol{r}) = \begin{pmatrix} 0 & 0 & \delta(\boldsymbol{r})Q & -\delta(\boldsymbol{r})Q^\dagger \\ 0 & 0 & \delta(\boldsymbol{r})Q & -\delta(\boldsymbol{r})Q^\dagger \\ Q^\dagger\delta(\boldsymbol{r}) & Q^\dagger\delta(\boldsymbol{r}) & 0 & 0 \\ -Q\delta(\boldsymbol{r}) & -Q\delta(\boldsymbol{r}) & 0 & 0 \end{pmatrix}, \tag{A1}$$

where the wave functions are written in the sublattice basis $\psi_{\boldsymbol{r}} = (a^K_{\boldsymbol{r}} \;\; a^{K'}_{\boldsymbol{r}} \;\; b^K_{\boldsymbol{r}} \;\; b^{K'}_{\boldsymbol{r}})^T$ and $Q^\dagger = k_x + ik_y$, $Q = k_x - ik_y$. Note that $\boldsymbol{r}, \boldsymbol{k}$ are (noncommuting) operators.

To find the symbol of $V(\boldsymbol{r}, \boldsymbol{k})$, we need to calculate its Weyl transform defined in Eq. (2). While this calculation is feasible, there is a simpler way to achieve the result. A property of the inverse Weyl transform, i.e., the Wigner transform, is that it transforms a classical Hamiltonian into its Weyl ordered quantum counterpart. The Weyl ordered Hamiltonian is obtained by complete symmetrization, e.g., $kr \to \frac{\hat{k}\hat{r}+\hat{r}\hat{k}}{2}$. We use it as follows. Each component in Eq. (A1) is written as a sum of a symmetric and an antisymmetric part with respect

to $\boldsymbol{k}$ and $\boldsymbol{r}$, e.g.,

$$\delta(\boldsymbol{r})Q = \frac{\{\delta(\boldsymbol{r}), Q\}}{2} + \frac{[\delta(\boldsymbol{r}), Q]}{2}, \tag{A2}$$

where $\{,\}$ and $[,]$ are respectively anticommutation and commutation relations. Since Q is linear in k_x, k_y the second term in Eq. (A2) is given by $\frac{-i(\partial_x - i\partial_y)\delta(\boldsymbol{r})}{2}$, i.e., it is a function of $\boldsymbol{r}$ only and not of $\boldsymbol{k}$, hence its symbol is given by replacing the operator $\hat{\boldsymbol{r}}$ by the parameter $\boldsymbol{r}$. The first term is Weyl ordered, so its Weyl symbol is given by the function $\delta(\boldsymbol{r})Q$, where $(\boldsymbol{r}, \boldsymbol{k})$ are parameters. Overall, using the standard notation $W[\cdots]$ for the symbol of an operator, we obtain

$$W[\delta(\boldsymbol{r})Q] = \delta(\boldsymbol{r})Q - \frac{i(\partial_x - i\partial_y)\delta(\boldsymbol{r})}{2}. \tag{A3}$$

Note that on the right hand side of Eq. (A3) $\boldsymbol{r}, \boldsymbol{k}$ are parameters, and will be so henceforth. Comparing the magnitude of the two terms in Eq. (A3), we have

$$\delta(\boldsymbol{r})Q - \frac{i(\partial_x - i\partial_y)\delta(\boldsymbol{r})}{2} \sim \frac{1}{2a}\delta(\boldsymbol{r})[(2k_x a - i) - i(2k_y a - i)], \tag{A4}$$

where a is the lattice constant. In the low energy limit $ka \ll 1$, the dominant term in Eq. (A3) is the second one that we keep. Moreover, using that $\delta(\boldsymbol{r})$ is a function of r only and not of θ, leads to

$$-i(\partial_x \pm i\partial_y)\delta(\boldsymbol{r}) = e^{\pm i\theta}\left(-i\partial_r \pm \frac{1}{r}\partial_\theta\right)\delta(\boldsymbol{r}) = -ie^{\pm i\theta}\partial_r\delta(\boldsymbol{r}). \tag{A5}$$

Overall, the symbol of the Hamiltonian of graphene with an A vacancy is the sum $W[H_0 + V(\boldsymbol{r}, \boldsymbol{k})]$, where the symbol of the unperturbed Hamiltonian H_0 in Eq. (5), is

$$W[H_0] = \begin{pmatrix} 0 & 0 & Q & 0 \\ 0 & 0 & 0 & -Q^\dagger \\ Q^\dagger & 0 & 0 & 0 \\ 0 & -Q & 0 & 0 \end{pmatrix}, \tag{A6}$$

namely the Bloch Hamiltonian [Eq. (6)]. The total symbol involves two types of terms, those which are function of $\boldsymbol{r}$ and those which are functions of $\boldsymbol{k}$ and $\boldsymbol{r}$. For the latter case, the $\boldsymbol{r}$-dependant part can be discarded. To see it, consider, e.g., the term

$$Q - \frac{ie^{-i\theta}\partial_r\delta(\boldsymbol{r})}{2}. \tag{A7}$$

The only contribution needed to extract relevant topology is the principle symbol of the Hamiltonian, obtained by considering only the highest order in $\boldsymbol{k}$ (highest order derivatives in the Hamiltonian) [23]. It is the first term in Eq. (A7), hence we can discard the second term. Notice that for the antidiagonal terms, this procedure does not apply since for them the principle symbol is given by $-ie^{\pm i\theta}\partial_r\delta(\boldsymbol{r})$, these terms being independent of $\boldsymbol{k}$.

Finally, we wish to emphasize that $\delta(\boldsymbol{r})$ is an approximation for the potential created by a vacancy. Generally, it can be replaced by some spatially localized function, whose exact shape is not important. Hence we take $\frac{\partial_r\delta(r)}{2} \to \phi(\boldsymbol{r})$. Together with the replacement $\theta \to \theta + \frac{\pi}{2}$ so as to absorb the $-i$ prefactor, we obtain

$$\mathcal{H}_V(\boldsymbol{k}, \boldsymbol{r}) = \begin{pmatrix} 0 & 0 & Q & e^{i\theta}\phi(r) \\ 0 & 0 & e^{-i\theta}\phi(r) & -Q^\dagger \\ Q^\dagger & e^{i\theta}\phi(r) & 0 & 0 \\ e^{-i\theta}\phi(r) & -Q & 0 & 0 \end{pmatrix} \tag{A8}$$

for the symbol of H_V, restoring the notations used in Eq. (9). This symbol when expressed in terms of Dirac matrices is

$$\mathcal{H}_V(\boldsymbol{k}, \boldsymbol{r}) = k_x\,\sigma_x \otimes \tau_z + k_y\,\sigma_y \otimes \mathbf{1} + \phi_1(\boldsymbol{r})\sigma_x \otimes \tau_x + \phi_2(\boldsymbol{r})\sigma_x \otimes \tau_y \tag{A9}$$

with $\phi_1(\boldsymbol{r}) + i\phi_2(\boldsymbol{r}) = \phi(r)\,e^{-i\theta}$ is the relation [Eq. (9)].

APPENDIX B: CONSTRUCTION OF THE TENFOLD WAY WITH THE SYMBOL

In this section we follow Ref. [5]. We work with Dirac symbols given by Eq. (11), of the form

$$\mathcal{H}(\boldsymbol{k}, \boldsymbol{r}) = \boldsymbol{h}_s(\boldsymbol{k}, \boldsymbol{r}) \cdot \boldsymbol{\gamma}_s + \boldsymbol{h}_a(\boldsymbol{k}, \boldsymbol{r}) \cdot \boldsymbol{\gamma}_a, \tag{B1}$$

where

$$\boldsymbol{h}_s(\boldsymbol{k}, \boldsymbol{r}) = \boldsymbol{h}_s(-\boldsymbol{k}, \boldsymbol{r}), \quad \boldsymbol{h}_a(\boldsymbol{k}, \boldsymbol{r}) = -\boldsymbol{h}_a(-\boldsymbol{k}, \boldsymbol{r}). \tag{B2}$$

We denote by p (resp. $q+1$) the number of γ_a (resp. γ_s). Momentum and position variables $\boldsymbol{k}$ and $\boldsymbol{r}$, are respectively defined by the d components $(k_1, \ldots, k_d)$ on the S^d sphere and the D spatial components $(r_1, \ldots, r_D)$ of the defect on S^D.

The purpose of this Appendix is to relate (p, q) to the symmetry class of a symbol indexed by s, namely to show that $s = p - q$. To that aim, the transition from one symmetry class to another is considered and then applied to Dirac symbols.

Starting from symbol in an s symmetry class, we show that by adding or removing one position or momentum coordinate, a new symbol can be constructed which belongs to another symmetry class. It is easy to see that there are exactly two types of mappings which either add or remove symmetries, namely increasing or decreasing s by one. We start from symmetry removing mappings. Consider a chiral symmetric symbol $\mathcal{H}_c$, namely anticommuting with the chirality operator C [Eq. (10)], and define the nonchiral symbol

$$\mathcal{H}_{nc} \equiv \cos\theta\,\mathcal{H}_c + \sin\theta\,C, \tag{B3}$$

where θ is position $(\boldsymbol{r})$ or momentum $(\boldsymbol{k})$-dependent coordinate, i.e., either D or d increases by 1. The second term in $\mathcal{H}_{nc}$ breaks chiral symmetry and consequently (for real classes) breaks either time reversal T or particle-hole P symmetry. To see which one is broken, we assume $[T, P] = 0$, so to rewrite the chirality operator as $C = i^{\frac{s-1}{2}}TP$ which squares to 1 for all odd values of s. Both T and P commute with C for $s = 1 \bmod 4$ and anticommute with C for $s = 3 \bmod 4$. From the symmetry requirements [Eq. (10)], time-reversal symmetry is broken for θ being a momentum coordinate and $s = 1 \bmod 4$ while particle-hole symmetry is broken for $s = 3 \bmod 4$, and

s increases by 1, and conversely if θ is a position dependent coordinate, s decreases by 1. Hence when s is odd

$$\mathcal{H}_c(s,d,D) \to \mathcal{H}_{nc}(s+1,d+1,D),$$
$$\mathcal{H}_c(s,d,D) \to \mathcal{H}_{nc}(s-1,d,D+1). \tag{B4}$$

Consider now a nonchiral symbol and build a chiral one by choosing

$$\mathcal{H}_c = \cos\theta\, \mathcal{H}_{nc} \otimes \sigma_z + \sin\theta\, \mathbf{1} \otimes \sigma_a \tag{B5}$$

where $a = x$ or $a = y$. This symbol has chiral symmetry since it anticommutes with $\mathbf{1} \otimes i\sigma_z\sigma_a$. The aim is now to choose a such that the new symbol preserves the original symmetry. This is also dependent on whether θ is momentum or position coordinate. For example if θ is a momentum (position) coordinate and $\mathcal{H}_{nc}$ has time reversal symmetry, we require $a = y(x)$. Now $\mathcal{H}_c$ has the additional symmetry $P = \sigma_x T(i\sigma_y T)$ that satisfies $P^2 = T^2(-T^2)$, implying $s \to s+1(s-1)$. A similar argument holds when $\mathcal{H}_{nc}$ possess particle-hole symmetry instead. Overall, we have thus showed that

$$\mathcal{H}_{nc}(s,d,D) \to \mathcal{H}_c(s+1,d+1,D),$$
$$\mathcal{H}_{nc}(s,d,D) \to \mathcal{H}_c(s-1,d,D+1). \tag{B6}$$

The mappings [Eqs. ((B4), (B6))] imply that for all s we have both

$$\mathcal{H}(s,d,D) \to \mathcal{H}(s+1,d+1,D),$$
$$\mathcal{H}(s,d,D) \to \mathcal{H}(s-1,d,D+1), \tag{B7}$$

namely that there is an homomorphism between symbols in class s and symbols in class $s+1$ or $s-1$ and in one dimension higher, either d or D. To show that these classes are isomorphic, an inverse map is required. The inverse map is more involved and we direct the reader to Ref. [5] for the thorough proof. By combining the mappings [Eq. (B7)], the symbols $\mathcal{H}(s,d,D)$ and $\mathcal{H}(s,d+1,D+1)$ become isomorphic, which implies that $\mathcal{H}(s,d,D) = \mathcal{H}(s,\delta)$ where $\delta = d - D$. The mappings in Eq. (B7) can now be simplified to

$$\mathcal{H}(s,\delta) = \mathcal{H}(s+1,\delta+1), \tag{B8}$$

which finally proves the scaling

$$\mathcal{H}(s,\delta) = \mathcal{H}(s-\delta) \tag{B9}$$

given in Eq. (14). This scaling is observed along the diagonal of the tenfold periodic classification as displayed by colors in Table I.

We now apply these results to Dirac symbols. Note that by design, if $\mathcal{H}_c$ is a Dirac symbol, i.e., it is build from anticommuting $\boldsymbol{\gamma}$ matrices, then C abides $\{\gamma_i, C\} = 0$ and $C^2 = 1$ so C is a γ matrix, and $\mathcal{H}_{nc}$ is also a Dirac symbol. If $\mathcal{H}_{nc}$ is a Dirac symbol, $\gamma_i \otimes \sigma_z$ are also γ matrices anticommuting with each other and with σ_a, so that $\mathcal{H}_c$ is a Dirac symbol. These results provide a systematic way to build higher dimension Dirac symbols for different s symmetry classes. Note that if θ is a momentum (position) coordinate then the second term is a γ_a (γ_s) matrix. The simplest Dirac symbol is $\mathcal{H}_0 = h_0(\boldsymbol{k},\boldsymbol{r})\gamma_s^0$ where $\gamma_s^0 = \mathbf{1}$ for which $p = q = 0$. It obviously possesses time reversal symmetry but no particle-hole symmetry so it is in *AI* class, i.e., with $s = 0$. Using the mappings [Eq. (B7)], it appears that higher dimension Dirac symbols can be obtained for all real classes as given by $s = p - q \bmod 8$. For example for $p = s$, $q = 0$ up to $s = 4$ [5].

[1] A. Altland and M. R. Zirnbauer, Phys. Rev. B **55**, 1142 (1997).
[2] A. Kitaev, AIP Conf. Proc. **1134**, 22 (2009).
[3] A. P. Schnyder, S. Ryu, A. Furusaki, and A. W. W. Ludwig, Phys. Rev. B **78**, 195125 (2008).
[4] M. Stone, C.-K. Chiu, and A. Roy, J. Phys. A: Math. Theor. **44**, 045001 (2011).
[5] J. C. Y. Teo and C. L. Kane, Phys. Rev. B **82**, 115120 (2010).
[6] G. Toulouse, and M. Kléman, J. Phys. Lett. **37**, 149 (1976).
[7] M. Kohmoto, Ann. Phys. **160**, 343 (1985).
[8] D. J. Thouless, M. Kohmoto, M. P. Nightingale, and M. den Nijs, Phys. Rev. Lett. **49**, 405 (1982).
[9] M. F. Atiyah and I. M. Singer, Bull. Am. Math. Soc. **69**, 422 (1963).
[10] M. F. Atiyah and I. M. Singer, Ann. Math. **87**, 484 (1968).
[11] M. Nakahara, *Geometry, Topology and Physics*, Graduate Student Series in Physics (Hilger, Bristol, 1990).
[12] M. Stone, Ann. Phys. **155**, 56 (1984).
[13] C.-K. Chiu, J. C. Y. Teo, A. P. Schnyder, and S. Ryu, Rev. Mod. Phys. **88**, 035005 (2016).
[14] C. Callias, Commun. Math. Phys. **62**, 213 (1978).
[15] Ìmit Ertem, J. Phys. Commun. **1**, 035001 (2017).
[16] T. Fukui, K. Shiozaki, T. Fujiwara, and S. Fujimoto, J. Phys. Soc. Jpn. **81**, 114602 (2012).
[17] T. Eguchi, P. B. Gilkey, and A. J. Hanson, Phys. Rep. **66**, 213 (1980).
[18] A. J. Niemi and G. W. Semenoff, Phys. Rev. D **30**, 809 (1984).
[19] E. Getzler, Commun. Math. Phys. **92**, 163 (1983).
[20] E. Akkermans, J. E. Avron, R. Narevich, and R. Seiler, Eur. Phys. J. B **1**, 117 (1998).
[21] M. Hillery, R. O'Connell, M. Scully, and E. Wigner, Phys. Rep. **106**, 121 (1984).
[22] W. B. Case, Am. J. Phys. **76**, 937 (2008).
[23] E. Yankowsky, A. Schwarz, and S. Levy, Quantum field theory and topology, *Grundlehren der mathematischen Wissenschaften* (Springer, Berlin, Heidelberg, 2013).
[24] A. H. Castro Neto, F. Guinea, N. M. R. Peres, K. S. Novoselov, and A. K. Geim, Rev. Mod. Phys. **81**, 109 (2009).
[25] K. Kelly and N. Halas, Surf. Sci. **416**, L1085 (1998).
[26] M. M. Ugeda, I. Brihuega, F. Guinea, and J. M. Gómez-Rodríguez, Phys. Rev. Lett. **104**, 096804 (2010).
[27] O. Ovdat, J. Mao, Y. Jiang, E. Y. Andrei, and E. Akkermans, Nat. Commun. **8**, 507 (2017).
[28] V. M. Pereira, F. Guinea, J. M. B. Lopes dos Santos, N. M. R. Peres, and A. H. Castro Neto, Phys. Rev. Lett. **96**, 036801 (2006).
[29] V. M. Pereira, J. M. B. Lopes dos Santos, and A. H. Castro Neto, Phys. Rev. B **77**, 115109 (2008).
[30] H. Amara, S. Latil, V. Meunier, P. Lambin, and J.-C. Charlier, Phys. Rev. B **76**, 115423 (2007).

[31] J. J. Palacios, J. Fernández-Rossier, and L. Brey, Phys. Rev. B **77**, 195428 (2008).
[32] C. Dutreix, L. Bilteanu, A. Jagannathan, and C. Bena, Phys. Rev. B **87**, 245413 (2013).
[33] Y. Abulafia, A. Goft, N. Orion, and E. Akkermans, arXiv:2307.05185.
[34] P. Mallet, I. Brihuega, S. Bose, M. M. Ugeda, J. M. Gómez-Rodríguez, K. Kern, and J. Y. Veuillen, Phys. Rev. B **86**, 045444 (2012).
[35] O. Ovdat, Y. Don, and E. Akkermans, Phys. Rev. B **102**, 075109 (2020).
[36] W. P. Su, J. R. Schrieffer, and A. J. Heeger, Phys. Rev. Lett. **42**, 1698 (1979).
[37] A. J. Heeger, S. Kivelson, J. R. Schrieffer, and W. P. Su, Rev. Mod. Phys. **60**, 781 (1988).
[38] C. Dutreix and M. I. Katsnelson, Phys. Rev. B **93**, 035413 (2016).
[39] B. R. K. Nanda, M. Sherafati, Z. S. Popović, and S. Satpathy, New J. Phys. **15**, 039501 (2013).
[40] C.-Y. Hou, C. Chamon, and C. Mudry, Phys. Rev. Lett. **98**, 186809 (2007).
[41] R. Jackiw and S.-Y. Pi, Phys. Rev. Lett. **98**, 266402 (2007).
[42] K. K. Gomes, W. Mar, W. Ko, F. Guinea, and H. C. Manoharan, Nature **483**, 306 (2012).
[43] A. C. Qu, P. Nigge, S. Link, G. Levy, M. Michiardi, P. L. Spandar, T. Matthé, M. Schneider, S. Zhdanovich, U. Starke, C. Gutiérrez, and A. Damascelli, Sci. Adv. **8**, eabm5180 (2022).
[44] C. Bao, H. Zhang, T. Zhang, X. Wu, L. Luo, S. Zhou, Q. Li, Y. Hou, W. Yao, L. Liu, P. Yu, J. Li, W. Duan, H. Yao, Y. Wang, and S. Zhou, Phys. Rev. Lett. **126**, 206804 (2021).
[45] S. Ryu and Y. Hatsugai, Phys. Rev. Lett. **89**, 077002 (2002).
[46] P. W. Brouwer, E. Racine, A. Furusaki, Y. Hatsugai, Y. Morita, and C. Mudry, Phys. Rev. B **66**, 014204 (2002).
[47] S. Ganeshan, K. Sun, and S. Das Sarma, Phys. Rev. Lett. **110**, 180403 (2013).
[48] E. H. Lieb, Phys. Rev. Lett. **62**, 1201 (1989).
[49] A. Venaille and P. Delplace, Phys. Rev. Res. **3**, 043002 (2021).